Cholecystokinin-A Signaling Regulates Automaticity of Pacemaker Cardiomyocytes and Shortens Sinus Node Recovery Time

Hongmei Ruan*, Ravi Mandla, Namita Ravi†, Giselle Galang, Amanda W. Soe, Jeffrey E. Olgin, Di Lang, and Vasanth Vedantham*

Cardiology Division, Department of Medicine and Cardiovascular Research Institute, University of California, San Francisco, CA

*co-corresponding authors

†Current Address: Yale University School of Medicine, 333 Cedar Street, New Haven, CT 06510

Short Title: CCK_AR Signaling in Pacemaker Cardiomyocytes

Corresponding Authors:

Hongmei Ruan, MD, PhD
Smith Cardiovascular Research Building
555 Mission Bay Blvd South, 314
San Francisco, CA 94158
hongmei.ruan@ucsf.edu

Vasanth Vedantham, MD, PhD
Smith Cardiovascular Research Building
555 Mission Bay Blvd South, 352M
San Francisco, CA 94158
TEL: 415-476-7559
FAX: 415-476-6260
vasanth.vedantham@ucsf.edu

Category: Original Article

Word Count: 7482 (not including title page)

ABSTRACT

Aims: The behavior of pacemaker cardiomyocytes (PCs) in the sinoatrial node (SAN) is modulated by neurohormonal and paracrine factors, many of which signal through G-protein coupled receptors (GPCRs). The aims of the present study are to catalog GPCRs that are differentially expressed in the mammalian SAN and to define the acute physiological consequences of activating the cholecystokinin-A signaling system in the SAN and in isolated PCs.

Methods and Results: Using bulk and single cell RNA sequencing datasets, we identify a set of GPCRs that are differentially expressed between SAN and right atrial tissue, including several whose roles in PCs and in the SAN have not been thoroughly characterized. Focusing on one such GPCR, Cholecystokinin-A receptor (CCK_AR), we demonstrate expression of *Cckar* mRNA specifically in mammalian PCs, and further demonstrate that subsets of SAN fibroblasts and neurons within the cardiac intrinsic nervous system express cholecystokinin, the ligand for CCK_AR. Using mouse models, we find that while baseline SAN function is not dramatically affected by loss of CCK_AR, the firing rate of individual PCs is slowed by exposure to sulfated cholecystokinin-8 (sCCK-8), the high affinity ligand for CCK_AR. The effect of sCCK-8 on firing rate is mediated by reduction in the rate of spontaneous phase 4 depolarization of PCs and is mitigated by activation of beta-adrenergic signaling. Finally, while perfusion of sCCK-8 onto the SAN *ex-vivo* reduces the beating rate modestly, exposure to sCCK-8 unexpectedly shortened the sinus node recovery time, a finding that has potential implications for treatment of SAN dysfunction.

Conclusions: (1) PCs express many GPCRs whose specific roles in SAN function have not been characterized, (2) the cholecystokinin-A pathway constitutes a novel signaling system that regulates SAN function and PC electrophysiology.

Translational Perspective

The time required for the sinoatrial node (SAN) to resume function after overdrive suppression is called the sinus node recovery time (SNRT). In the tachy-brady syndrome, pathological prolongation of the SNRT results in symptomatic sinus pauses that follow the termination of a tachyarrhythmia, leading to loss of consciousness. Tachy-brady syndrome is the most common presentation of sinus node dysfunction and can only be treated with a permanent pacemaker. In this study, we find that activation of the cholecystokinin-A signaling system can shorten the SNRT, raising the possibility of developing new pharmacological methods to treat tachy-brady syndrome.

1. INTRODUCTION

The sinoatrial node (SAN) contains an electrotonically coupled network of pacemaker cardiomyocytes (PCs) that depolarizes the atrial myocardium to initiate the heartbeat. Cellular automaticity in PCs is driven by mutual entrainment of hyperpolarization-activated cyclic nucleotide gated ion channels ("membrane clock") and spontaneous subsarcolemmal calcium release ("calcium clock") [1]. PCs are also densely innervated with sympathetic [2] and post-ganglionic parasympathetic nerve fibers [3], the latter originating within the ganglia of the cardiac intrinsic nervous system (CINS). In addition, paracrine signals from fibroblasts and macrophages, tissue stretch, and humoral input all influence the firing rate of PCs and impulse transmission from the SAN to the atrium. Incorporation of PCs and their complex responses into a patterned network allows the SAN to function as a robust and tunable rhythm generator for the heart.

Sinus node dysfunction (SND) is a common heart rhythm disorder that causes activity intolerance, dizziness, and fainting. The most common clinical manifestation of SND is "tachy-brady" syndrome, in which atrial tachyarrhythmias occur in paroxysms that terminate with long sinus pauses before resumption of normal rhythm. Importantly, the prolongation of sinus node recovery time (SNRT) in tachy-brady syndrome reflects a loss of robustness in SAN function that is distinct from SAN chronotropic response though the two are often impaired in patients with SND. Nevertheless, drugs that can shorten SNRT, including beta-adrenergic agonists or phosphodiesterase inhibitors, are catecholaminergic and therefore increase heart rate and contractility, potentiate tachyarrhythmias, and produce systemic effects, rendering them nonviable as long-term therapies for SND. On the other hand, drugs that are used to treat tachyarrhythmias typically prolong SNRT and necessitate the implantation of permanent pacemakers to prevent pauses. Non-sympathomimetic pharmacological approaches to long term management of SND do not currently exist.

In this context, it is noteworthy that the complexity of interactions between PCs and their various inputs are only beginning to be unraveled. While the model of mutual antagonism between sympathetic input via norepinephrine and parasympathetic input via acetylcholine explains much SAN behavior, other neurotransmitters and modulators, operating both within the CINS as well as at the CINS-SAN interface, are relevant to SAN function [4]. Supporting the notion of additional pathways relevant to heart rate regulation, recent genome-wide expression studies by our group and other groups have highlighted the enrichment of mRNA encoding several neurotransmitters and neurotransmitter receptors within the CINS and SAN whose specific roles are not well understood, in addition to numerous G-protein coupled receptors (GPCRs) that are differentially expressed in PCs as compared to atrial cardiomyocytes. While physiological roles and functional consequences have been assigned to some of these pathways, many remain uncharacterized.

Here, we survey the landscape of differentially expressed GPCRs in PCs and explore the cholecystokinin signaling pathway, which has not been well characterized in the SAN although its components have been identified in the heart from early stages of cardiac development [5]. In the peripheral nervous system, in numerous organs and tissues, and in the brain, activation of cholecystokinin A receptor (CCK_AR) by sulfated cholecystokinin octapeptide (sCCK-8), its highest affinity agonist, results in signaling via the heterotrimeric G proteins (typically Gq/11 or Gs) with diverse downstream effects, including induction of gene expression, enzyme secretion, promotion of satiety, natriuresis, and a host of other important physiological consequences [6]. However, much less is known about potential roles for CCK_A signaling in the heart. One prior study found that administration of sCCK-8 to isolated rat hearts results in heart rate slowing that persists despite autonomic blockade [7], while a separate study found that low-dose sCCK-8 led to tachycardia in rat hearts while high dose sCCK-8 induced bradycardia [8], suggesting a potentially complex mechanism of action on heart rhythm. However, the possibility of a specific chronotropic effect of cholecystokinin on PCs has not yet been demonstrated, nor has it been determined how activation of this pathway might be relevant to impulse generation and propagation within the isolated SAN.

In the present work, we mine existing mRNA expression datasets to demonstrate that *Cckar* is among the most differentially expressed GPCRs between murine SAN and right atrial cardiomyocytes [9]. We further explore scRNA-seq datasets to define the specific SAN cell populations that express *Cckar* and its ligand, CCK. We then use cellular electrophysiology and optical mapping of SAN tissue in WT and $Cckar^{-/-}$ mice to assess acute physiological responses to activation of the CCK_AR signaling pathway in the mouse heart, which include modest heart rate slowing and, unexpectedly, shortening of the sinus node recovery time. Taken together, our data demonstrate a novel signaling axis between the CINS, SAN fibroblasts, and PCs that can regulate mammalian sinus node function, with potential relevance to the most common form of sinus node dysfunction.

2. METHODS

A detailed methods section is available in the Supplementary Materials.

2.1 Animal Handling and Maintenance

Mouse studies were performed in accordance with IACUC-approved protocols at the University of California, San Francisco. $Cckar^{tm1Kpn}$ (hereafter, $Cckar^{-/-}$) mice were generated by Alan Kopin et al. and were obtained from Nirao Shah's lab [10]. $Cck^{tm1.1(cre)Zjh}$ (hereafter, Cck^{Cre}) mice were obtained from Jackson Labs. $Gt(ROSA)26Sor^{tm4(ACTB\text{-}tdTomato,\text{-}EGFP)Luo}$ (hereafter, $ROSA^{mT/mG}$) mice were generated by Muzumdar et al. and were obtained from Brian Black's lab [11].

2.2 Analysis of Gene Expression

Bulk RNA sequencing data was generated by Vedantham et al. [9] and Galang et al. [12] and downloaded from the Gene Expression Omnibus (GEO, GSE65658 and GSE148515, respectively), while mouse E16.5 SAN single-cell RNA-sequencing data were generated by Goodyer et al. [13] and downloaded from GEO (GSE132658). Adult rabbit single-cell RNA-seq data were generated by Liang et al. [14] and were downloaded as fastq files from the NCBI Sequence Read Archive (PRJNA531288). Quantitative PCR was performed using Taqman Probes (Thermo Fisher) with GAPDH as an endogenous control using the ΔΔCT method for comparison of SAN and right atrial tissue. Immunostaining and acetylcholinesterase staining were performed as previously described and are detailed in the Supplementary Methods.

2.3 Transmitter Implantation and Analysis of Heart Rhythm Data

Adult mice (8-12 weeks old) underwent subcutaneous implantation of telemetry devices (ETA-F10, Data Science International, MN) under anesthesia according to the manufacturer's instructions. Heart rhythm analysis was performed offline using Ponemah (Data Sciences International, St Paul, MN). 48 hours of heart rhythm data were analyzed for each mouse. Time-domain, frequency-domain, and arrhythmia analysis were performed as previously described[15] with modifications detailed in the Supplementary Methods.

2.4 Whole Cell Patch Clamp

Adult mouse pacemaker cells were isolated for recording as previously described [12] and as detailed in the Supplementary Methods. Action potentials were acquired from spontaneously beating adult cells of the indicated genotypes via the perforated patch-clamp technique with an Axopatch-700B amplifier using pCLAMP10.3. The pCLAMP 10.6 Clampfit module and LabChart7 were used for analysis of action potentials (APs) as detailed in the Supplementary Methods.

2.5 *Ex-vivo* Optical Mapping and Electrophysiology Studies

Isolated atrial preparations of wild type (WT, n = 8) and *Cckar*$^{-/-}$ (n = 5) mice were prepared as previously described and as detailed in the Supplementary Methods.[16] The membrane potential probe RH237 (5 μl, 1.25 mg/ml, Invitrogen, Carlsbad, CA), Ca^{2+} probe Rhod-2 AM (5 μl, 1.25 mg/ml, Invitrogen, Carlsbad, CA) [17] were applied to the sinus node area, bounded by the superior vena cava, inferior vena cava, crista terminalis (lateral), and interatrial septum (medial). Membrane potential and Ca^{2+} signals were collected during baseline conditions and after superfusion of 1 nM sCCK-8 (Tocris Bioscience, Minneapolis, MN) and were analyzed as described in the Supplementary Methods. To measure the corrected sinus node recovery time (cSNRT), the timing from the last pacing stimulus to

the first spontaneous beat was measured after burst pacing at a rate of 10 Hz for 30 seconds. The spontaneous cycle length from subtracted from the post-pacing interval to yield the cSNRT.

3 RESULTS

3.1 Differential GPCR Expression in the Sinoatrial Node

To identify GPCRs that might regulate SAN function, we analyzed a previously published bulk RNA sequencing dataset generated by our lab that was derived from sorted neonatal mouse PCs and right atrial cardiomyocytes (RACMs) [12]. Differentially expressed GPCRs were identified by intersecting the list of expressed genes in both PCs and RACMs with an annotated list of GPCRs obtained from the International Union of Basic and Clinical Pharmacology[18]. We identified a total of 71 GPCRs expressed in PCs or RACMs, of which 29 were enriched in RACMs, 22 enriched in the PCs, and 29 expressed in both based on a false discovery rate of 0.2 (Supplementary Figure 1, Supplementary Tables 1-3). Among the list of GPCRs enriched in PCs were receptors for canonical regulators of SAN function including adenosine (*Adora1*) and norepinephrine (*Adra1b*), as well as enrichment of receptors with ligands that do not have established associations with SAN function, such as lysophosphatidic acid (*Lpar3*) and phoenixin (*Gpr173*), orphan GPCRs (*Gpr22*, *Gpr85*, *Gpr157*, and *Gpr27*), adhesion GPCRs (*Adgrb2, Adgrd1*), and an opsin (Opn3). A third category of GPCRs included those whose ligands are known to affect SAN function but via mechanisms that have not been fully characterized. This group includes receptors for ligands that are reported to acutely increase heart rate such as glucagon (*Gcgr*) [19], pituitary adenylate cyclase activating polypeptide (*Adcyap1r1*) [20], prostaglandin $F_{2\alpha}$ (*Ptgfr*) [21], and thromboxane A2 (*Tbx2ar*) [22]; receptors whose ligands are reported to acutely decrease heart rate including sphingosine 1-phosphate (*S1pr3*) [23] and somatostatin (*Sstr4*) [24], and one ligand for highly expressed GPCR for which there exists prior conflicting data on acute physiological responses, cholecystokinin (*Cckar*). Given the unclear effects of cholecystokinin-A signaling in the PCs, and its high degree of differential expression with RACMs, we sought to define the role of this signaling pathway in more detail.

3.2 Cckar and Other GPCRs are Expressed in Sinoatrial Node Pacemaker Cells

To define the expression pattern of *Cckar* in the SAN at different time points, we explored publicly available RNAseq datasets of adult and embryonic SAN tissue. When the SAN was micro-dissected using laser capture, *Cckar* mRNA was highly enriched in SAN compared to right atrial tissue at embryonic day (E)14.5, postnatal day (P)4, and at 2 weeks of age (Figure 1A-C). Additional RNA sequencing datasets derived from sorted cells enriched for pacemaker cells also confirmed expression of *Cckar* in late embryonic and neonatal murine SAN (Figure 1B). To test whether *Cckar* is expressed in adult SAN tissue, SAN tissue and right atrial tissue were dissected from 3 adult hearts and *Cckar*

mRNA was quantified using GAPDH as an endogenous control. *Cckar* mRNA was detected in all SAN samples but in none of the RA samples (Figure 1C).

The SAN contains pacemaker cells, atrial cardiomyocytes, fibroblasts, and other cell types, so to establish whether *Cckar* expression is restricted to pacemaker cells or is also expressed in other SAN cell populations, we explored recently published single cell RNA sequencing datasets derived from murine and rabbit sinoatrial node. Datasets were clustered using UMAP and cell populations identified by expression of established marker genes (Figure 1D). A pacemaker cell cluster was identified that co-expressed *Hcn4* and *Isl1* (Figure 1E, F). Examination of *Cckar* expression within the *Hcn4*$^{+}$/*Isl1*$^{+}$ pacemaker cell cluster revealed high and differential expression as compared to other cell types. (Figure 1G, H and Supplementary Figure 2), confirming the presence of *Cckar* transcript specifically in mouse and rabbit cardiac pacemaker cells.

3.3 CCK-expressing neurons and fibroblasts are present in the SAN

Because sCCK-8 is produced by many cell types and can function via endocrine signaling pathways as well as via neurotransmission, we hypothesized that sCCK-8 might be produced within the cells of the cardiac intrinsic nervous system that project to the SAN or in other cardiac cell types near pacemaker cells. The scRNA-seq datasets described above demonstrated that *Cck* transcript was observed in both SAN fibroblasts and within a subset of cardiac neurons lying within the SAN (Figure 2A, B). To test further whether we could observe evidence of *Cck* expression in these cell types, we crossed *Cck*^{cre} mice, in which *Cre recombinase* is inserted downstream of the endogenous *Cck* gene using an internal ribosomal entry site, with *ROSA*^{mTmG} reporter mice, in which membrane targeted GFP is expressed upon recombination by Cre. Thus, GFP^{+} cells in *CCK-cre; ROSA*^{mTmG} represent cells that have expressed *Cck* for sufficient duration and in sufficient quantity to recombine a reporter allele at the *ROSA* locus.

Consecutive frozen sections from 1 month old *Cck*^{cre}*; ROSA*^{mTmG} hearts were visualized under direct fluorescence and stained with acetyl cholinesterase (AChE), a marker for ganglionated plexi (Figure 2C). Adjacent sections demonstrated GFP+ neurons with the right atrial ganglionated plexus (Figure 2D, E). In addition, GFP+ cellular projections were observed to course within the SAN but did not overlap with Hcn4 expression, a marker of cardiac pacemaker cells (Figure 2F-H). The morphology and locations of these projections suggest neuronal identity. In addition to these projections, we also observed several Hcn4^{-} non-myocyte cells that were green fluorescent, with morphologies consistent with fibroblasts (Figure 2I-K). Taken together, the imaging and scRNA-seq data support the conclusions that CCK-producing neurons are present within the heart and project to the SAN and that the SAN contains CCK-expressing fibroblasts. Importantly, these data establish that either the CINS or native SAN fibroblasts (or both) could serve as sources of ligand for Cckar expressed on cardiac pacemaker cells.

3.4 Sinoatrial Node Function in *Cckar*$^{-/-}$ Mice

To test whether CCK_AR is required for SAN pacemaking under ordinary conditions, we assessed heart rhythm and activity using implanted transmitters in *Cckar*$^{-/-}$ mice (*n*=11, 8 male and 3 female) in comparison with WT littermates (n=7, 5 male and 2 female). EKG tracings from both groups of mice were similar with no significant differences in average RR, PR, or QRS intervals (Figure 3A, Supplementary Figure 3A-E). With respect to diurnal variation in heart rate, the *Cckar*$^{-/-}$ mice exhibited a modest slowing of average heart rate, particularly during waking hours (high activity period) (Figure 3B). Notably, activity counts were also reduced in the *Cckar*$^{-/-}$ mice during similar periods. (Figure 3C). Both intrinsic heart rate (determined after administration of atropine and propranolol) and maximum heart rate (determined after isoproterenol infusion) were similar between *Cckar*$^{-/-}$ mice and WT littermates (Figure 3D, E). When heart rate was collated into 10 beat-per-minute bins and plotted in a histogram, there was a modest shift to slightly slower heart rates during high activity periods in the knockout mice (Figure 3F). For each mouse, we also counted sinus pauses, episodes of sinus bradycardia, and episodes of AV block over 48 hours of continuous recording and found no significant differences in arrhythmia frequency between WT and *Cckar*$^{-/-}$ mice (Supplementary Figure 3F-H). Finally, we assessed heart rate variability in *Cckar*$^{-/-}$ mice in the time domain by estimating RMSSD, SDRR, and pNN6 during low activity periods, and did not observe any significant differences between the two groups of mice (Supplementary Figure 4A-F). Frequency domain analysis revealed a small increase in low frequency power in *Cckar*$^{-/-}$ mice without significant differences in total power or in high and frequency contributions to the power spectra (Supplementary Figure 4G-J).

3.5 sCCK-8 slows spontaneous firing in isolated adult PCs

To test whether sCCK-8 affects electrophysiological properties of PCs, we isolated PCs from adult WT C57Bl6 mice and measured action potentials in whole cell current clamp mode using the perforated patch technique. Individual mouse pacemaker cells were exposed to different concentrations of sCCK-8 during AP recording. In the presence of 1nM isoproterenol, commonly used in isolated PCs to approximate behavior under physiological sympathetic tone, perfusion of sCCK-8 slowed firing rate (Figure 4A, B). The onset of the effect varied but generally occurred within one minute of exposure and was largely complete by 3 minutes. Firing rate did not recover to baseline after washing out the sCCK-8. None of the PCs isolated from adult *Cckar*$^{-/-}$ mice exposed to 5 nM and 10 nM sCCK-8 exhibited an effect on firing rate, demonstrating that the negative chronotropic effect of sCCK-8 requires the presence of CCK_AR (Figure 4C, D). The effect size was largely dosage-independent, with 10-20% slowing of firing rate at dosages of 2.5 nM (*n*=7), 5 nM (*n* = 13), and 10nM (*n*=13) of s-CCK-8, and a non-significant effect observed at 1nM (*n*=5). (Figure 4E, F). Notably, a subset of spontaneously firing

PCs did not respond to s-CCK8, as reflected in the broad distribution of percentage change in firing rate.

Considering the small effect size and high variability from cell-to-cell, we hypothesized that isoproterenol might have blunted the negative chronotropic response to sCCK-8, so we repeated these experiments using 5 nM sCCK-8 in the absence of isoproterenol. As expected, we observed a larger and consistent negative chronotropic effect of 5 nM sCCK-8 on firing rate without isoproterenol present, suggesting that sCCK-8 and isoproterenol activate pathways with opposing effects on the determinants of firing rate (Figure 5).

To better define the electrophysiological mechanism for the reduction in firing rate, AP morphology was quantified in the presence of sCCK-8 in the presence and absence of isoproterenol. Action potential duration at 50% repolarization (APD50, msec), actional potential amplitude (mV), maximum diastolic potential (MDP, mV), takeoff potential (TOP, mV), and early diastolic depolarization (EDDR, mV/msec) were determined at baseline and after perfusion with 5 or 10 nM sCCK-8. Of these parameters, we observed reductions in EDDR and an increase in APD50 in the presence of sCCK-8, suggesting a signaling mechanism that reduced spontaneous depolarization and affected repolarization without significantly affecting other components of the pacemaker cell action potential (Figure 5). The decrease in EDDR also occurred in the presence of isoproterenol, although the effect was less pronounced (Supplementary Figure 5). Importantly, we did not observe changes in AP morphology in PCs from *Cckar*$^{-/-}$ mice exposed to sCCK-8, again underscoring the dependence of the pharmacological effect on the expression of CCK_AR.

3.6 sCCK-8 Slows SAN Rate, Displaces the Site of the Leading Pacemaker, and Shortens SAN Recovery Time

To test for the effect of sCCK-8 on SAN activation at the tissue level, we performed optical mapping on isolated intact perfused WT and *Cckar*$^{-/-}$ SAN (Figure 6A). Addition of 1 nM or 5 nM s-CCK8 to the perfusate resulted in prolongation of the basic cycle length in 4/5 WT SAN preparations but had no effect on SAN tissue from *Cckar*$^{-/-}$ mice (Figure 6B, C). We also recorded the site of origin of the leading pacemaker within the SAN before and after perfusion of sCCK-8. The leading pacemaker in WT preparations shifted after sCCK-8 administration by an average of 0.63 ± 0.03 mm as compared to 0.24 ± 0.03 mm in *Cckar*$^{-/-}$ hearts ($p < 0.0001$) (Figure 6D, E). Of note, we did not observe a consistent direction of pacemaker migration, as is typically observed after administration of adrenergic agonists (cranial shift) or cholinergic agonists (caudal shift).

Finally, we tested whether perfusion of sCCK-8 affected the sinus node recovery time. To do this, isolated SAN-atrial preparations were paced for 30 seconds at 10Hz and the time from the last pacing stimulus to the first sinus impulse was recorded (Figure 7A). The pre-pacing cycle length was subtracted from this quantity to yield the corrected sinus node recovery time (cSNRT). We observed a

significant and reproducible reduction in cSNRT after perfusion with 1 nM and with 5 nM sCCK-8 in WT preparations (Figure 7B). As expected, *ex-vivo* SAN preparations from *Cckar*$^{-/-}$ mice did not exhibit any change in cSNRT, demonstrating that this effect depended on the expression of CCK_AR. Pacing also resulted in a shift in the site of origin of the leading pacemaker in the setting of sCCK-8 in WT but not in *Cckar*$^{-/-}$ mice, demonstrating that activation of the cholecystokinin signaling pathway affects tissue-level behavior of the SAN (Figure 7C).

4 DISCUSSION

Our main findings are (1) mammalian PCs express functional CCK_AR, (2) CINS neurons and SAN fibroblasts express CCK, (3) sCCK-8 slows PC and SAN firing rate by reducing the slope of early diastolic depolarization, and (4) sCCK shortens the sinus node recovery time. Taken together, these data provide evidence for a novel signaling system in PCs that affects mammalian SAN function through direct effects on automaticity and on SAN robustness to overdrive suppression.

4.1 GPCR Expression in the SAN

Analysis of existing RNA sequencing datasets identified several GPCRs that are enriched in SAN tissue and expressed in both SAN and atrial tissue, including orphan GPCRs and GPCRs with defined ligands but no known functions in regulating heart rhythm. Ligands for several of these GPCRs, including *Sstr4*, *S1pr3*, *Gcgr*, and *Adcyap1r1* trigger defined chronotropic responses but the molecular mechanisms driving their specific actions on isolated pacemaker cells have been characterized only for some[25]. Our findings of high-level and differential expression of these receptors in PCs suggest that chronotropic responses to these ligands are mediated by direct effects on PC automaticity. Further work will be required to define the specific electrophysiological effects of these signaling pathways on PCs in physiological contexts and to identify the relevant sources of their ligands. Importantly, leading computational models of the PC action potential have yet to incorporate dynamic signaling through simultaneously activated receptors for these various ligands, and the potential roles of these signaling pathways in long-term versus short-term SAN physiology have not been determined. The catalog of GPCRs presented here could form a foundation for such efforts and for deeper exploration of interaction between the CINS and SAN beyond the canonical signaling pathways involved in autonomic regulation of the heartbeat.

4.2 Expression of Cholecystokinin Signaling Pathway Components in the SAN

Recent studies have explored the functional neuroanatomy of the cardiac intrinsic nervous system with particular attention to innervation of the SAN. In a recent single cell qPCR analysis of porcine heart, CCK-expressing neurons were identified as a subset of right atrial ganglionated plexus

neurons and included cells that projected directly to the SAN [26]. Using a *Cck*^{Cre} mouse line to drive reporter gene expression, we uncovered similar findings in mice, with Cre-expressing neurons observed in the RAGP and in projections within the SAN, findings that we confirmed with analysis of scRNA-seq data. An additional finding of note is the presence of CCK-expressing fibroblasts within the SAN which has not been previously described and raises the possibility of paracrine signaling from SAN fibroblasts to pacemaker cells. The stimulus for secretion and whether such signaling might play a role in sinus node dysfunction remain to be determined. However, the deep conservation of expression of the CCK signaling system among mammals suggests a conserved functional role in SAN function and in autonomic regulation of heart rhythm.

4.3 Role of Cholecystokinin Signaling in Regulating Heart Rhythm

Cckar$^{-/-}$ mice had slower heart rates than WT mice, particularly during high activity periods. However, because CCK_AR is involved in many central and peripheral neuronal and organ-specific signaling pathways, the changes in heart rate might not reflect a change in intrinsic sinus node function, but rather a change in heart rates caused by other CCK_AR -dependent physiological processes. For example, reduced activity in *Cckar*$^{-/-}$ mice could have led to the slower heart rates, although we cannot exclude the opposite possibility that compromised SAN function reduced activity levels. However, our finding that *Cckar*$^{-/-}$ mice do not exhibit sinus node dysfunction or changes in intrinsic heart rate after autonomic blockade suggests that CCK_AR signaling is not required for SAN function under baseline conditions in adult mice. Related to this point, the magnitude of the sCCK-8 effect on isolated pacemaker cells is modest as assessed on a short time scale and could be counteracted by co-administration of isoproterenol, suggesting that the primary role of this pathway in autonomic regulation of SAN function may not be direct beat-to-beat regulation of heart rate. Alternatively, there may be redundant mechanisms that mitigate the loss of CCK_AR in *Cckar*$^{-/-}$mice. In future work, development of conditional mouse model in which loss of CCK_AR is restricted to PCs could be used to better define the PC- and SAN-autonomous roles of CCK_AR signaling in heart rhythm regulation.

4.4 Acute effects of Cckar Signaling on Isolated Pacemaker Cells

Several studies in rodent models have demonstrated that injection of sCCK-8 into an anesthetized animal or bolus injection of sCCK-8 to the heart *ex-vivo* can produce changes in heart rate. Our work confirms these results and extends the earlier findings by demonstrating that sCCK-8 acutely and directly reduces the firing rate of PCs by lowering the EDDR and lengthening the APD. While CCK_AR is generally considered to signal preferentially via Gq [27], signaling via Gs [28], Gi [29], or G12/13 [30, 31] has been reported in different cellular contexts. Of note, activation of Gq specifically in murine SAN PCs using a genetically encoded optogenetic tool *increased* heart rate by ~5% [32], while activation of Gq using DREADD technology resulted in a non-significant increase in heart rate [33],

suggesting that the acute decrease in firing rate we observed may not result purely from signaling via Gq. In the present study we did not attempt to elucidate the signaling downstream of CCK_AR that results in the reduction of firing rate, but the reduction in EDDR could theoretically result from reduction in cyclic adenosine monophosphate (cAMP) levels as might be expected with signaling via Gi. The finding that the magnitude of the effect could be blunted by co-administration of isoproterenol, an activator of Gs, would support such a hypothesis.

4.5 Potential Relevance to Human SAN Dysfunction and Tachy-Brady Syndrome

A striking finding of the present study is the reduction in corrected sinus node recovery time that we observed in response to sCCK-8 exposure in *ex-vivo* SAN preparations. In general, cSNRT shortens under conditions of high sympathetic tone or in response to treatment with sympathomimetic agents. However, these agents also increase heart rate and can worsen atrial tachyarrhythmias. Similarly, although natriuretic peptide receptor C (NPR-C) agonists have shown promise in rescuing both bradycardia and cSNRT prolongation in models of SAN disease – primarily by preventing the development of fibrosis over long time scales [34] –acute heart rate increases are also observed in response to NPR-C agonists[35]. In contrast, sCCK-8 shortens cSNRT without exerting a dramatic effect on heart rate, thereby decoupling chronotropy from SAN robustness to overdrive pacing. The molecular basis for this effect may be distinct from the effects of sCCK-8 on action potential morphology and on firing rate of individual PCs. One possible mechanism could involve regulation of electrotonic interactions among SAN cells, resulting in more robust SAN function despite the modest reduction in firing rate of individual cells. Another possibility could involve ligand-induced switching of PCs from a non-firing mode to a firing mode, which could improve the robustness of the SAN to overdrive suppression [36]. Ultimately, determining the mechanistic basis for how sCCK-8 shortens cSNRT without increasing heart rate could be relevant to developing new approaches to tachy-brady syndrome, a condition in which prolonged SNRT results in sinus pauses and fainting spells.

4.6 Limitations

Our study does not directly address the possibility that CCK_AR signaling affects SAN properties not related to acute physiological response. In addition, we used a global loss of function model, which confounds our ability to define the physiological consequences of perturbing CCK_AR signaling specifically in PCs. Despite these limitations, the present study demonstrates functional expression of CCK_AR in PCs and establishes a foundation for future work on this signaling pathway and its relevance to heart rhythm regulation.

Funding: This work was supported by the National Institutes of Health [grant number DP2HL152425 to V.V.]; the American Heart Association [Career Development Award 846898 to D.L.]; and the Sarnoff Cardiovascular Research Foundation [Research Fellowship to N.R.].

Acknowledgements: The authors are grateful to Huiliang Qui for assistance with preparing materials for optical mapping, and to Gagandeep Chouhan for assistance with genotyping and mouse colony management.

Conflict of Interest: V.V. received consulting fees from Merck and research funding from Amgen, neither of which are related to the research presented in this article.

REFERENCES

1. Lakatta EG, Maltsev VA, Vinogradova TM. A coupled system of intracellular ca2+ clocks and surface membrane voltage clocks controls the timekeeping mechanism of the heart's pacemaker. *Circ Res*. 2010;**106**:659-673

2. Kimura K, Ieda M, Fukuda K. Development, maturation, and transdifferentiation of cardiac sympathetic nerves. *Circ Res*. 2012;**110**:325-336

3. Rysevaite K, Saburkina I, Pauziene N, Noujaim SF, Jalife J, Pauza DH. Morphologic pattern of the intrinsic ganglionated nerve plexus in mouse heart. *Heart Rhythm*. 2011;**8**:448-454

4. MacDonald EA, Rose RA, Quinn TA. Neurohumoral control of sinoatrial node activity and heart rate: Insight from experimental models and findings from humans. *Front Physiol*. 2020;**11**:170

5. Leigh RS, Ruskoaho HJ, Kaynak BL. Cholecystokinin peptide signaling is regulated by a tbx5-mef2 axis in the heart. *Peptides*. 2021;**136**:170459

6. Dufresne M, Seva C, Fourmy D. Cholecystokinin and gastrin receptors. *Physiol Rev*. 2006;**86**:805-847

7. Marker JD, Roberts ML. Chronotropic actions of cholecystokinin octapeptide on the rat heart. *Regul Pept*. 1988;**20**:251-259

8. Zhao XY, Ling YL, Meng AH, Shan BE, Zhang JL. Effects of cholecystokinin octapeptide on rat cardiac function and the receptor mechanism. *Sheng Li Xue Bao*. 2002;**54**:239-243

9. Vedantham V, Galang G, Evangelista M, Deo RC, Srivastava D. Rna sequencing of mouse sinoatrial node reveals an upstream regulatory role for islet-1 in cardiac pacemaker cells. *Circulation research*. 2015;**116**:797-803

10. Kopin AS, Mathes WF, McBride EW, Nguyen M, Al-Haider W, Schmitz F, Bonner-Weir S, Kanarek R, Beinborn M. The cholecystokinin-a receptor mediates inhibition of food intake yet is not essential for the maintenance of body weight. *J Clin Invest*. 1999;**103**:383-391

11. Muzumdar MD, Tasic B, Miyamichi K, Li L, Luo L. A global double-fluorescent cre reporter mouse. *Genesis*. 2007;**45**:593-605

12. Galang G, Mandla R, Ruan H, Jung C, Sinha T, Stone NR, Wu RS, Mannion BJ, Allu PKR, Chang K, Rammohan A, Shi MB, Pennacchio LA, Black BL, Vedantham V. Atac-seq reveals an isl1 enhancer that regulates sinoatrial node development and function. *Circ Res*. 2020;**127**:1502-1518

13. Goodyer WR, Beyersdorf BM, Paik DT, Tian L, Li G, Buikema JW, Chirikian O, Choi S, Venkatraman S, Adams EL, Tessier-Lavigne M, Wu JC, Wu SM. Transcriptomic profiling of the developing cardiac conduction system at single-cell resolution. *Circulation Research*. 2019;**125**:379-397

14. Liang D, Xue J, Geng L, Zhou L, Lv B, Zeng Q, Xiong K, Zhou H, Xie D, Zhang F, Liu J, Liu Y, Li L, Yang J, Xue Z, Chen YH. Cellular and molecular landscape of mammalian sinoatrial node revealed by single-cell rna sequencing. *Nat Commun*. 2021;**12**:287

15. Fenske S, Probstle R, Auer F, Hassan S, Marks V, Pauza DH, Biel M, Wahl-Schott C. Comprehensive multilevel in vivo and in vitro analysis of heart rate fluctuations in mice by ecg telemetry and electrophysiology. *Nat Protoc*. 2016;**11**:61-86

16. Lang D, Medvedev RY, Ratajczyk L, Zheng J, Yuan X, Lim E, Han OY, Valdivia HH, Glukhov AV. Region-specific distribution of transversal-axial tubule system organization underlies heterogeneity of calcium dynamics in the right atrium. *Am J Physiol Heart Circ Physiol*. 2022;**322**:H269-H284

17. Lang D, Sato D, Jiang Y, Ginsburg KS, Ripplinger CM, Bers DM. Calcium-dependent arrhythmogenic foci created by weakly coupled myocytes in the failing heart. *Circ Res*. 2017;**121**:1379-1391

18. Alexander SPH, Christopoulos A, Davenport AP, Kelly E, Mathie A, Peters JA, Veale EL, Armstrong JF, Faccenda E, Harding SD, Pawson AJ, Sharman JL, Southan C, Davies JA, Collaborators C. The concise guide to pharmacology 2019/20: G protein-coupled receptors. *Br J Pharmacol*. 2019;**176** Suppl 1:S21-S141

19. Mukharji A, Drucker DJ, Charron MJ, Swoap SJ. Oxyntomodulin increases intrinsic heart rate through the glucagon receptor. *Physiol Rep*. 2013;**1**:e00112

20. Hoover DB, Girard BM, Hoover JL, Parsons RL. Pac(1) receptors mediate positive chronotropic responses to pacap-27 and vip in isolated mouse atria. *Eur J Pharmacol*. 2013;**713**:25-30

21. Courtney KR, Colwell WT, Jensen RA. Prostaglandins and pacemaker activity in isolated guinea pig sa node. *Prostaglandins*. 1978;**16**:451-459

22. Takayama K, Yuhki K, Ono K, Fujino T, Hara A, Yamada T, Kuriyama S, Karibe H, Okada Y, Takahata O, Taniguchi T, Iijima T, Iwasaki H, Narumiya S, Ushikubi F. Thromboxane a2 and prostaglandin f2alpha mediate inflammatory tachycardia. *Nat Med*. 2005;**11:**562-566

23. Guo J, MacDonell KL, Giles WR. Effects of sphingosine 1-phosphate on pacemaker activity in rabbit sino-atrial node cells. *Pflugers Arch*. 1999;**438**:642-648

24. Bubinski R, Kus W, Goch J. [effect of somatostatin on the conduction system of the heart]. *Kardiol Pol*. 1993;**38**:258-262

25. Sanna MG, Vincent KP, Repetto E, Nguyen N, Brown SJ, Abgaryan L, Riley SW, Leaf NB, Cahalan SM, Kiosses WB, Kohno Y, Brown JH, McCulloch AD, Rosen H, Gonzalez-Cabrera PJ. Bitopic sphingosine 1-phosphate receptor 3 (s1p3) antagonist rescue from complete heart

block: Pharmacological and genetic evidence for direct s1p3 regulation of mouse cardiac conduction. *Mol Pharmacol*. 2016;**89**:176-186

26. Moss A, Robbins S, Achanta S, Kuttippurathu L, Turick S, Nieves S, Hanna P, Smith EH, Hoover DB, Chen J, Cheng ZJ, Ardell JL, Shivkumar K, Schwaber JS, Vadigepalli R. A single cell transcriptomics map of paracrine networks in the intrinsic cardiac nervous system. *iScience*. 2021;**24**:102713

27. Liu Q, Yang D, Zhuang Y, Croll TI, Cai X, Dai A, He X, Duan J, Yin W, Ye C, Zhou F, Wu B, Zhao Q, Xu HE, Wang MW, Jiang Y. Ligand recognition and g-protein coupling selectivity of cholecystokinin a receptor. *Nat Chem Biol*. 2021;**17**:1238-1244

28. Wu V, Yang M, McRoberts JA, Ren J, Seensalu R, Zeng N, Dagrag M, Birnbaumer M, Walsh JH. First intracellular loop of the human cholecystokinin-a receptor is essential for cyclic amp signaling in transfected hek-293 cells. *J Biol Chem*. 1997;**272**:9037-9042

29. Scemama JL, Robberecht P, Waelbroeck M, De Neef P, Pradayrol L, Vaysse N, Christophe J. Cck and gastrin inhibit adenylate cyclase activity through a pertussis toxin-sensitive mechanism in the tumoral rat pancreatic acinar cell line ar 4-2j. *FEBS Lett*. 1988;**242**:61-64

30. Sabbatini ME, Bi Y, Ji B, Ernst SA, Williams JA. Cck activates rhoa and rac1 differentially through galpha13 and galphaq in mouse pancreatic acini. *Am J Physiol Cell Physiol*. 2010;**298**:C592-601

31. Le Page SL, Bi Y, Williams JA. Cck-a receptor activates rhoa through g alpha 12/13 in nih3t3 cells. *Am J Physiol Cell Physiol*. 2003;**285**:C1197-1206

32. Wagdi A, Malan D, Beauchamp JS, Naryanan UBS, Dusend V, Sasse P, Bruegmann T. Opn5 a new optogenetic receptor to study gq signalling in the heart with light. *EP Europace*. 2021;**23**:euab116.574

33. Kaiser E, Tian Q, Wagner M, Barth M, Xian W, Schroder L, Ruppenthal S, Kaestner L, Boehm U, Wartenberg P, Lu H, McMillin SM, Bone DBJ, Wess J, Lipp P. Dreadd technology reveals major impact of gq signalling on cardiac electrophysiology. *Cardiovasc Res*. 2019;**115**:1052-1066

34. Mackasey M, Egom EE, Jansen HJ, Hua R, Moghtadaei M, Liu Y, Kaur J, McRae MD, Bogachev O, Rafferty SA, Ray G, Kirkby AW, Rose RA. Natriuretic peptide receptor-c protects against angiotensin ii-mediated sinoatrial node disease in mice. *JACC Basic Transl Sci*. 2018;**3**:824-843

35. Springer J, Azer J, Hua R, Robbins C, Adamczyk A, McBoyle S, Bissell MB, Rose RA. The natriuretic peptides bnp and cnp increase heart rate and electrical conduction by stimulating ionic currents in the sinoatrial node and atrial myocardium following activation of guanylyl cyclase-linked natriuretic peptide receptors. *J Mol Cell Cardiol*. 2012;**52**:1122-1134

36. Fenske S, Hennis K, Rotzer RD, Brox VF, Becirovic E, Scharr A, Gruner C, Ziegler T, Mehlfeld V, Brennan J, Efimov IR, Pauza AG, Moser M, Wotjak CT, Kupatt C, Gonner R, Zhang R, Zhang H, Zong X, Biel M, Wahl-Schott C. Camp-dependent regulation of hcn4 controls the tonic entrainment process in sinoatrial node pacemaker cells. *Nat Commun*. 2020;**11**:5555

FIGURE LEGENDS

Figure 1. Cckar is Expressed in Mouse Cardiac Pacemaker Cells. (A) Read counts for Cckar from Bulk RNA sequencing of sinoatrial node (SAN) tissue and right atrial tissue isolated from 3 embryonic day 14.5 Hcn4-GFP BAC transgenic mouse embryos using laser capture microdissection (original dataset from Ref. [9]) (B) Read counts for *Cckar* from Bulk RNA sequencing of sorted Hcn4-GFP+ pacemaker cells and atrial cardiomyocytes from neonatal mouse hearts shown in the heatmap (C) quantitative PCR for Cckar mRNA in samples manually dissected from adult mouse SAN and right atrium, using GAPDH as an endogenous control (n = 3 biological replicates). (D) Uniform Manifold Approximation Projection (UMAP) plot of leiden clustering analysis of single cell RNA sequencing data derived from 6 E16.5 mouse embryonic heart tissue samples taken from the SAN region demonstrated a pacemaker cell population (red circle, cluster 11), marked by co-expression of *Hcn4* (E) and *Isl1* (F), as well as several other identifiable cell types (original dataset from ref [12]). Cckar was differentially expressed in the pacemaker cluster (C11), as seen in the UMAP plot (G) and in the violin plot (H).

Figure 2. Expression of Cck in Neurons and Cardiac Fibroblasts. (A) Uniform Manifold Approximation and Projection (UMAP) plot of a single cell RNA sequencing dataset from neonatal sinoatrial node (SAN) (Ref [12]) demonstrates expression of *Cck* in a population of fibroblasts and in a cardiac neuron, as seen in the magnified images in panel (B). Adjacent serial sections from a neonatal *Cck-Cre;ROSA*^{mTmG} mouse heart stained with acetylcholinesterase to mark the right atrial cardiac ganglion (C) or imaged with epifluorescence to visualize Td-tomato and GFP expression (D,E) demonstrate that GFP+ cells, representing Cck expressing cells, are detectable in neuronal cell bodies within the ganglia. Sectioning and epifluorescence visualization of the SAN *Cck-Cre;ROSA*^{mTmG} showed few GFP+ cells (F) but as shown in (G) and (H), GFP+ axons could be observed coursing alongside Hcn4+ pacemaker cells (white arrowheads). Notably, GFP expression did not overlap with Hcn4 expression. A nearby section from the SAN (I) also revealed GFP+ cells with fibroblast morphologies in the SAN that did not express Hcn4 (J, K – yellow arrowheads).

Figure 3. Heart Rhythm in *Cckar*$^{-/-}$ Mice. (A) Electrocardiographic (ECG) tracings from awake unrestrained WT (top, black) and *Cckar*$^{-/-}$ (bottom, red) adult mice. (B) Diurnal heart rate variation among 7 WT and 11 *Cckar*$^{-/-}$adult mice implanted with ECG transmitters. Each point shows mean +/- SEM. (C) Activity counts for 7 WT and 11 *Cckar*$^{-/-}$adult mice implanted with transmitters. Each point shows mean +/- SEM. (D) Heart rate before (baseline) and after atropine and propranolol injection (A/P) in 7 WT (black) and 9 *Cckar*$^{-/-}$mice (red). Error bars denote standard deviation. (E) Heart rate before (baseline) and after isoproterenol injection (Max) in 5 WT (black) and 6 *Cckar*$^{-/-}$ mice (red). Error bars denote standard deviation.

(F) Averaged histograms of heart rate during low activity period (left) and high activity period (right) in 7 WT (black) and 11 *Cckar*$^{-/-}$mice (red) with 10 beat per minute bins.

Figure 4. sCCK-8 Reduces Spontaneous Firing Rate of Pacemaker Cells. (A) Spontaneous firing rate for an isolated adult WT pacemaker cell before and during perfusion of 5 mM sCCK-8, and after washout. (B) Superimposed spontaneous action potentials from an adult WT pacemaker cell firing spontaneously at baseline (solid line) and after perfusion with 10 nM sCCK-8 (dashed line). (C) Spontaneous firing rate for an isolated adult *Cckar*$^{-/-}$ pacemaker cell before and during perfusion with 5 nM sCCK-8. (D) Superimposed spontaneous action potentials from an adult *Cckar*$^{-/-}$ pacemaker cell at baseline (solid line) and during perfusion with 10 mM sCCK-8 (dashed line). (D) Change in spontaneous firing rate of (E) adult WT (n = 6) and (F) adult *Cckar*$^{-/-}$ (n = 9) pacemaker cells at baseline (BL) and 1 minute after perfusion of 10 nM sCCK-8. Statistical comparison was made with a paired T-test. (F) Percent change in spontaneous firing rate for individual adult WT pacemaker cells 1 minute after perfusion of 1 nM (n=5), 2.5 nM (n=7), 5 nM (n=7), 10 nM (n=6), or 20 nM (n=4) sCCK-8. (G) Percent change in firing rate in single adult *Cckar*$^{-/-}$ pacemaker cells before and after perfusion with 5 nM (n=9) or 10 nM (n=9) sCCK-8. Error bars indicate standard deviation.

Figure 5. sCCK-8 Reduces Early Spontaneous Depolarization in Pacemaker Cardiomyocytes. (A) Slowing of spontaneous firing in response to sCCK-8 perfusion in a WT pacemaker cardiomyocyte (PC) in the absence of isoproterenol (B) Lack of response of a PC from a Cckar-/- SAN (C). Definition of action potential parameters. The top tracing, $V_m(t)$, shows spontaneous action potentials (APs) from an isolated adult pacemaker cell and the bottom tracing shows the first derivative (*dV/dt*). The minimum diastolic potential (MDP) was defined as the minimum potential recorded between action potentials; Take off potential (TOP) was defined as the membrane potential at which dV/dt reach 10% of its maximum value; and early diastolic depolarization rate (EDDR) was defined as the average value of *dV/dt* over the shaded area in the bottom panel (from 10% to 50% of the MDP-to-TOP interval). (D) AP parameters including Firing Rate, Amplitude, APD_{50}, MDP, TOP, and EDDR were measured under baseline conditions in WT and *Cckar*$^{-/-}$ PCs (n = 8 and n = 5, respectively), and 3 minutes after perfusion with 5 nM sCCK-8. Statistical comparisons between baseline values and between pre- and post-sCCK-8 values were made with nonparametric tests (ns, non-significant, '*' $P < 0.05$, '**', $P < 0.01$).

Figure 6. sCCK-8 Acutely Prolongs SAN Cycle Length *ex-vivo*. (A) Micrograph demonstrating the *ex vivo* preparation used for optical mapping. (B) Percentage change in basic cycle length of *ex-vivo* SAN preparation assessed with optical mapping before (time 0) and at 0.5, 1, 2, 3, and 5 minutes after superfusion with 1nM sCCK-8. Dashed lines indicate responses of each individual preparation, and the

solid line shows the average response (*n* = 5). (C) Same as (B) but with preparations taken from *Cckar*$^{-/-}$ hearts (*n* = 5). (D) Cartoon diagram of *ex-vivo* preparation demonstrating migration of the the leading pacemaker from before superfusion with 1nM sCCK-8 (open circles) to after (solid circles) (*n* = 5). (E) Same as (D) but for *Cckar*$^{-/-}$ preparations (*n* = 5). Abbreviations: RAA, right atrial appendage; SVC, superior vena cava; IVC, inferior vena cava; SAN, sinoatrial node; LAA, left atrial appendage; RV, right ventricle; LV, left ventricle; IAS, interatrial septum.

Figure 7. sCCK-8 Reduces SAN Recovery Time. (A) Sinus node recovery time (SNRT) in WT (top panel) and *Cckar*$^{-/-}$ (bottom panel) SAN preparations assessed with optical action potential recording before, during, and after a 30-second 10 Hz pacing train. SNRT was measured as the time from the final pacing stimulus to first return beat under baseline conditions (blue tracing) and in the presence of 1 nM sCCK-8 (red tracing). (B) Corrected SNRT was calculated by subtracting the baseline cycle length pre-pacing from the SNRT under baseline conditions (BSL), 1 nM sCCK-8, 5 nM sCCK-8 in WT (top panel) and *Cckar*$^{-/-}$ SAN preparations (bottom panel). (C) Assessment of the site of the leading pacemaker using activation timing of optical action potentials under baseline conditions (blue) and after perfusion with 1 nM sCCK-8 (red) in WT and *Cckar*$^{-/-}$ SAN preparations. The dashed blue line indicates the level of the site of the leading pacemaker, which shifts cranially in WT SAN after sCCK-8 perfusion but not under other conditions. Abbreviations: RAA, right atrial appendage; SVC, superior vena cava; IVC, inferior vena cava; SAN, sinoatrial node; LAA, left atrial appendage; CT, crista terminalis; IAS, interatrial septum.

Figure 1

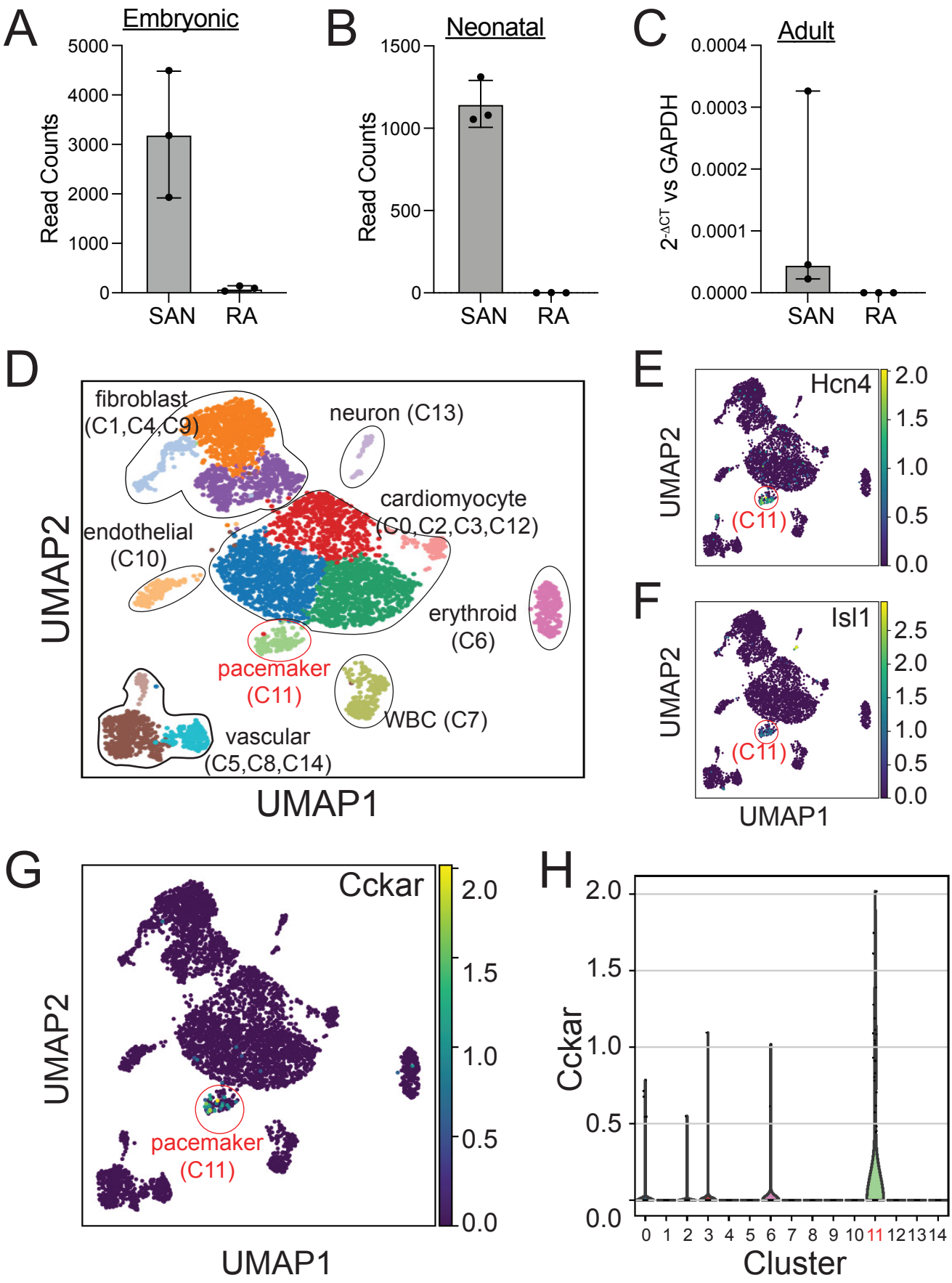
A
Embryonic
Read Counts
5000
4000
3000
2000
1000
0
SAN
RA
B
Neonatal
Read Counts
1500
1000
500
0
SAN
RA
C
Adult
2^-ΔCT vs GAPDH
0.0004
0.0003
0.0002
0.0001
0.0000
SAN
RA
D
fibroblast
(C1,C4,C9)
neuron (C13)
cardiomyocyte
(C0,C2,C3,C12)
endothelial
(C10)
erythroid
(C6)
pacemaker
(C11)
WBC (C7)
vascular
(C5,C8,C14)
UMAP2
UMAP1
E
Hcn4
(C11)
UMAP2
2.0
1.5
1.0
0.5
0.0
F
Isl1
(C11)
UMAP2
UMAP1
2.5
2.0
1.5
1.0
0.5
0.0
G
Cckar
pacemaker
(C11)
UMAP2
UMAP1
2.0
1.5
1.0
0.5
0.0
H
Cckar
2.0
1.5
1.0
0.5
0.0
0 1 2 3 4 5 6 7 8 9 10 11 12 13 14
Cluster

Figure 2

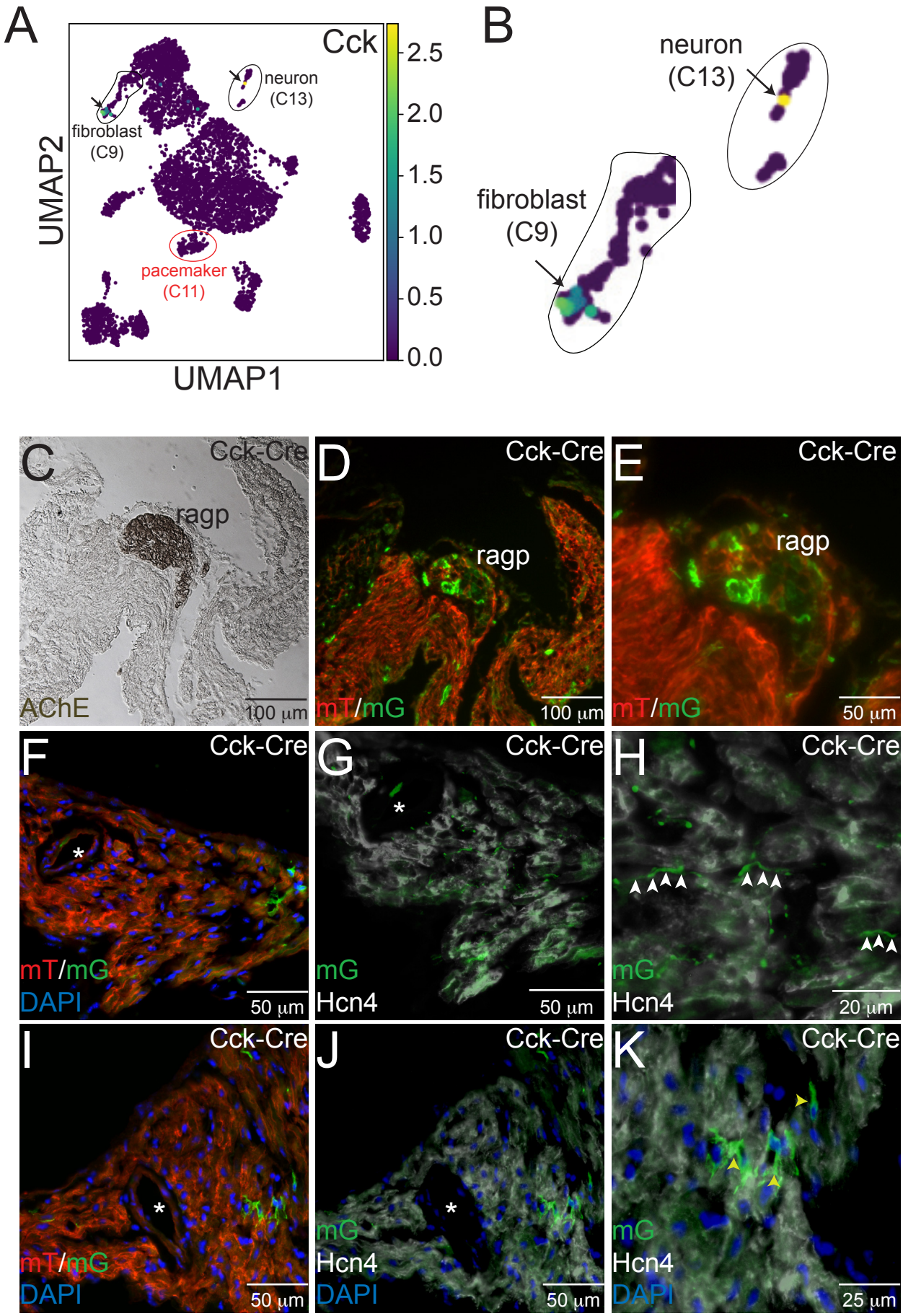
A
Cck
neuron
(C13)
fibroblast
(C9)
pacemaker
(C11)
UMAP2
UMAP1
2.5
2.0
1.5
1.0
0.5
0.0
B
neuron
(C13)
fibroblast
(C9)
C
Cck-Cre
ragp
AChE
100 µm
D
Cck-Cre
ragp
mT/mG
100 µm
E
Cck-Cre
ragp
mT/mG
50 µm
F
Cck-Cre
mT/mG
DAPI
50 µm
G
Cck-Cre
mG
Hcn4
50 µm
H
Cck-Cre
mG
Hcn4
20 µm
I
Cck-Cre
mT/mG
DAPI
50 µm
J
Cck-Cre
mG
Hcn4
DAPI
50 µm
K
Cck-Cre
mG
Hcn4
DAPI
25 µm

Figure 3

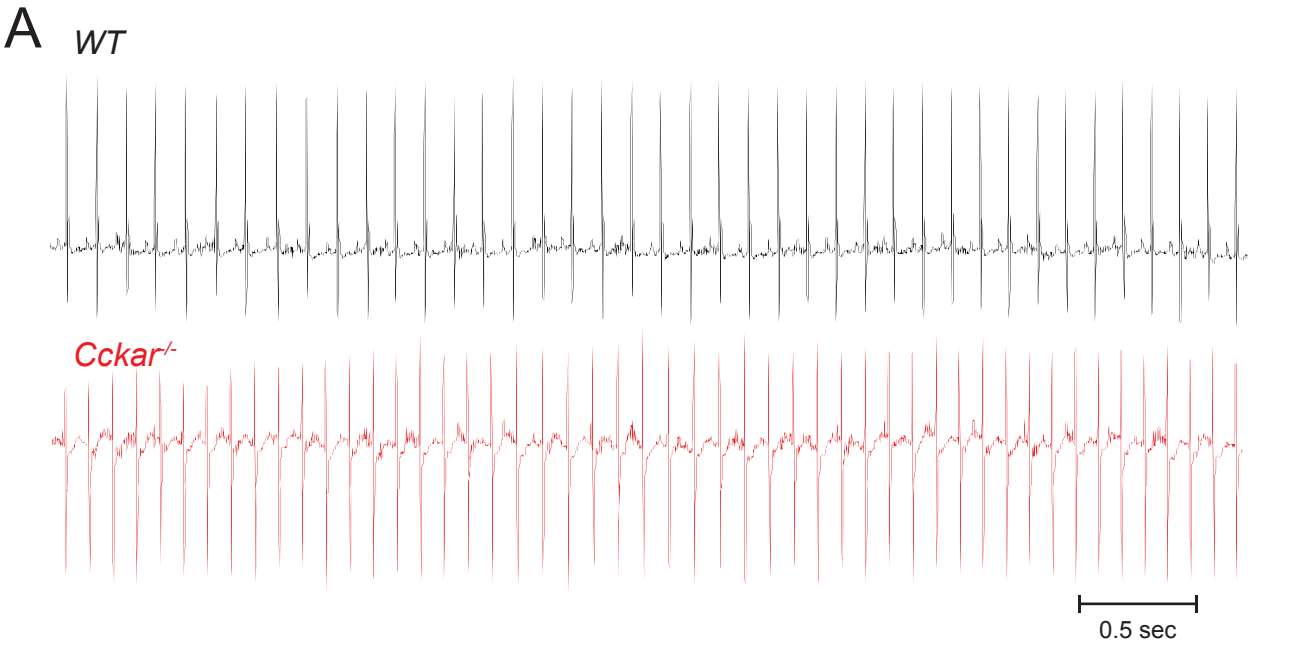
A
WT
Cckar-/-
0.5 sec

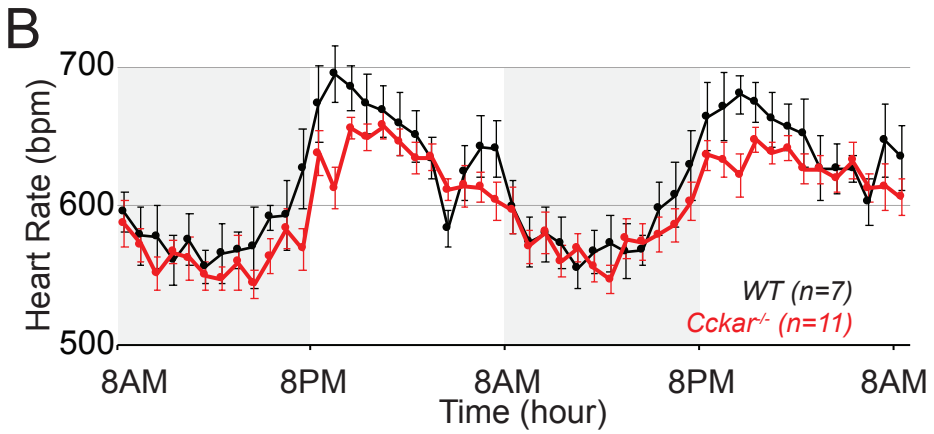
B
Heart Rate (bpm)
700
600
500
8AM
8PM
8AM
8PM
8AM
Time (hour)
WT (n=7)
Cckar-/- (n=11)

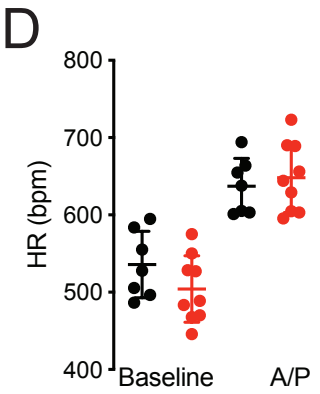
D
HR (bpm)
800
700
600
500
400
Baseline
A/P

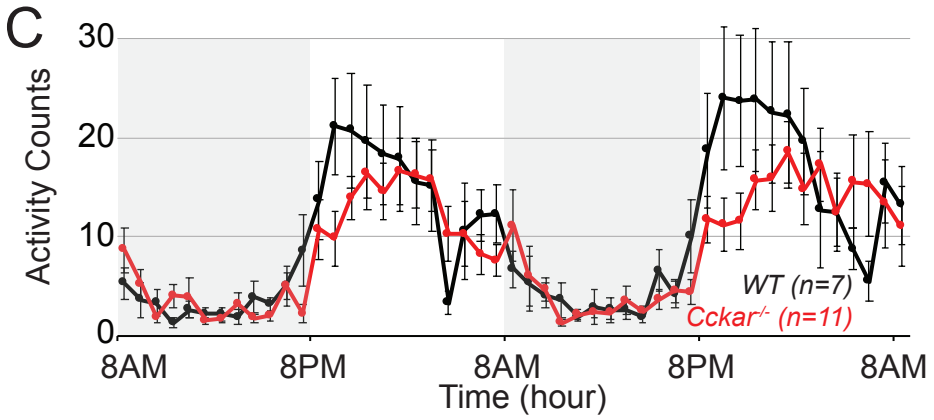
C
Activity Counts
30
20
10
0
8AM
8PM
8AM
8PM
8AM
Time (hour)
WT (n=7)
Cckar-/- (n=11)

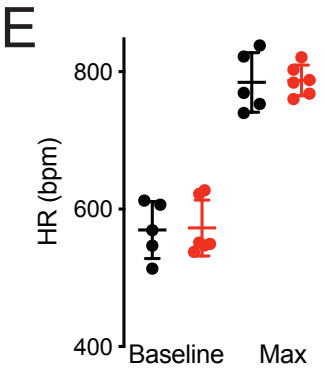
E
HR (bpm)
800
600
400
Baseline
Max

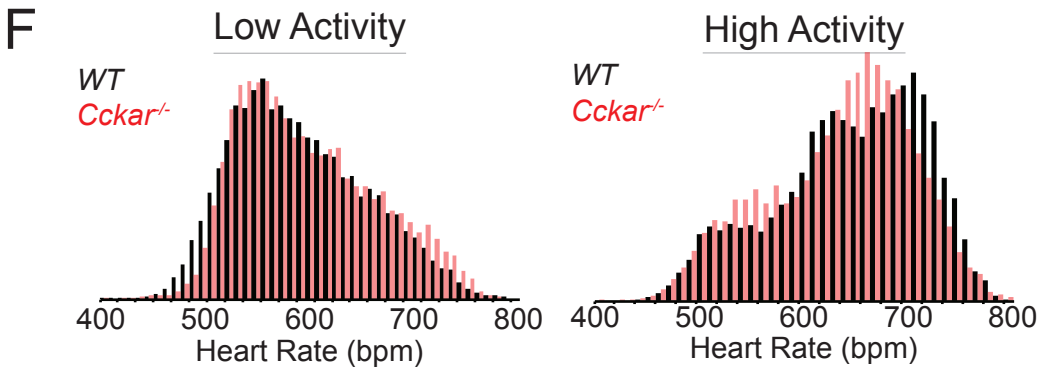
F
Low Activity
WT
Cckar-/-
400
500
600
700
800
Heart Rate (bpm)
High Activity
WT
Cckar-/-
400
500
600
700
800
Heart Rate (bpm)

Figure 4

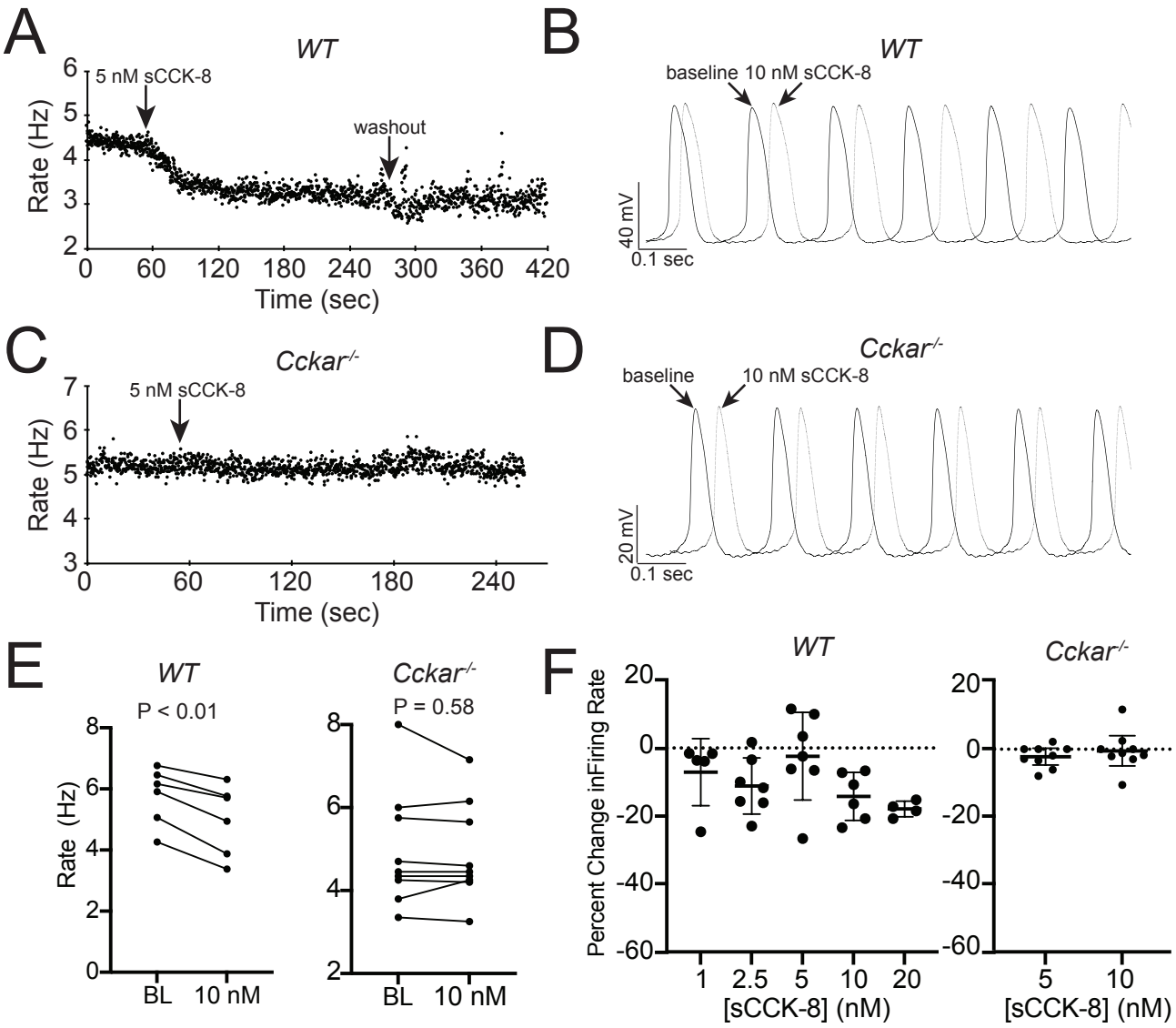
A
WT
5 nM sCCK-8
washout
Rate (Hz)
Time (sec)
B
WT
baseline 10 nM sCCK-8
40 mV
0.1 sec
C
Cckar-/-
5 nM sCCK-8
Rate (Hz)
Time (sec)
D
Cckar-/-
baseline
10 nM sCCK-8
20 mV
0.1 sec
E
WT
P < 0.01
Cckar-/-
P = 0.58
Rate (Hz)
BL
10 nM
F
WT
Cckar-/-
Percent Change inFiring Rate
[sCCK-8] (nM)

Figure 5

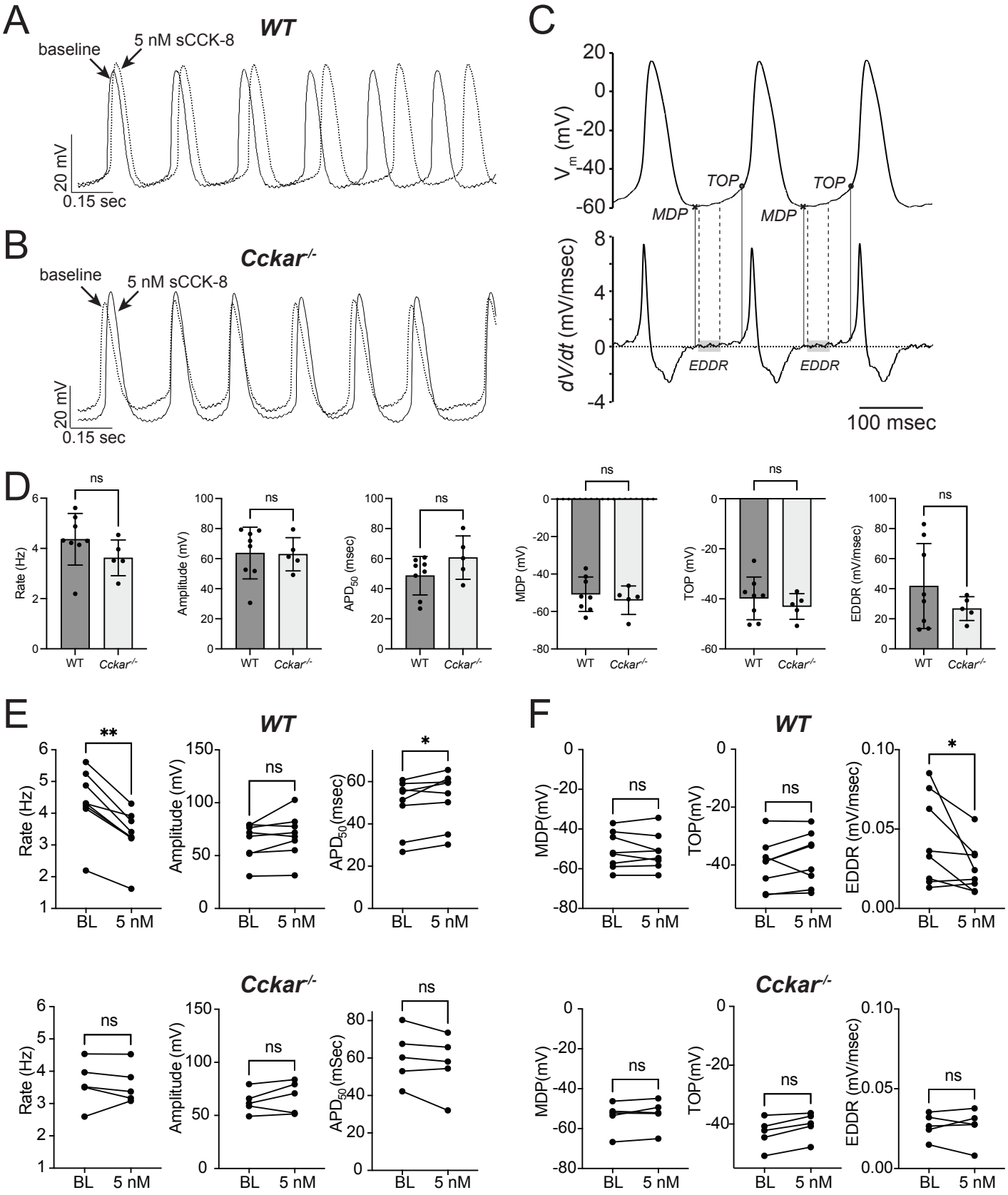
A
WT
baseline
5 nM sCCK-8
20 mV
0.15 sec
B
Cckar-/-
baseline
5 nM sCCK-8
20 mV
0.15 sec
C
Vm (mV)
TOP
MDP
dV/dt (mV/msec)
EDDR
100 msec
D
Rate (Hz)
Amplitude (mV)
APD50 (msec)
MDP (mV)
TOP (mV)
EDDR (mV/msec)
ns
WT
Cckar-/-
E
WT
Cckar-/-
Rate (Hz)
Amplitude (mV)
APD50 (msec)
APD50 (mSec)
BL
5 nM
**
*
ns
F
WT
Cckar-/-
MDP(mV)
TOP(mV)
EDDR (mV/msec)
BL
5 nM
*
ns

Figure 6

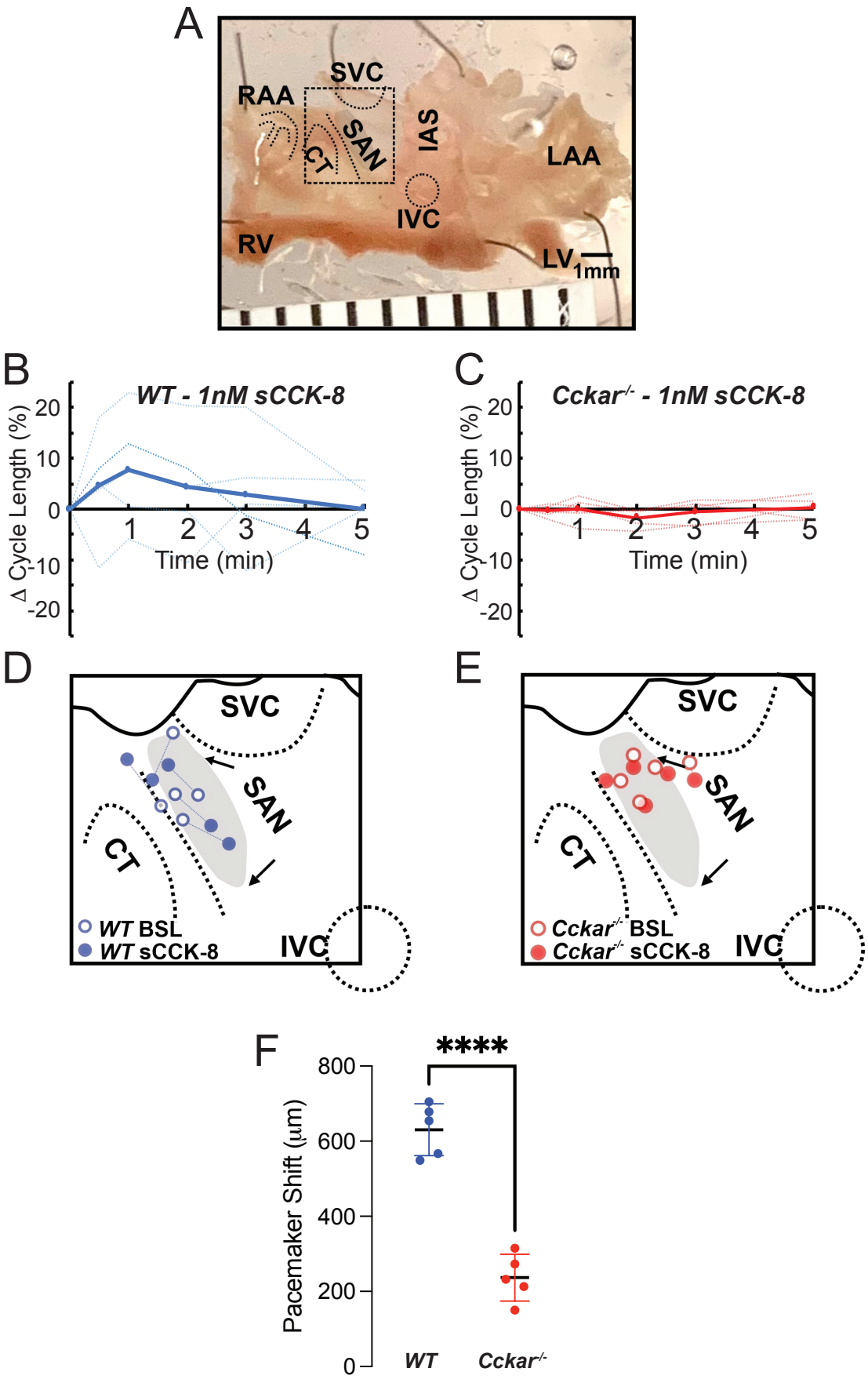
A
SVC
RAA
SAN
CT
IAS
LAA
IVC
RV
LV
1mm
B
WT - 1nM sCCK-8
Δ Cycle Length (%)
20
10
0
-10
-20
1
2
3
4
5
Time (min)
C
Cckar-/- - 1nM sCCK-8
Δ Cycle Length (%)
20
10
0
-10
-20
1
2
3
4
5
Time (min)
D
SVC
SAN
CT
IVC
WT BSL
WT sCCK-8
E
SVC
SAN
CT
IVC
Cckar-/- BSL
Cckar-/- sCCK-8
F
****
Pacemaker Shift (µm)
800
600
400
200
0
WT
Cckar-/-

Figure 7

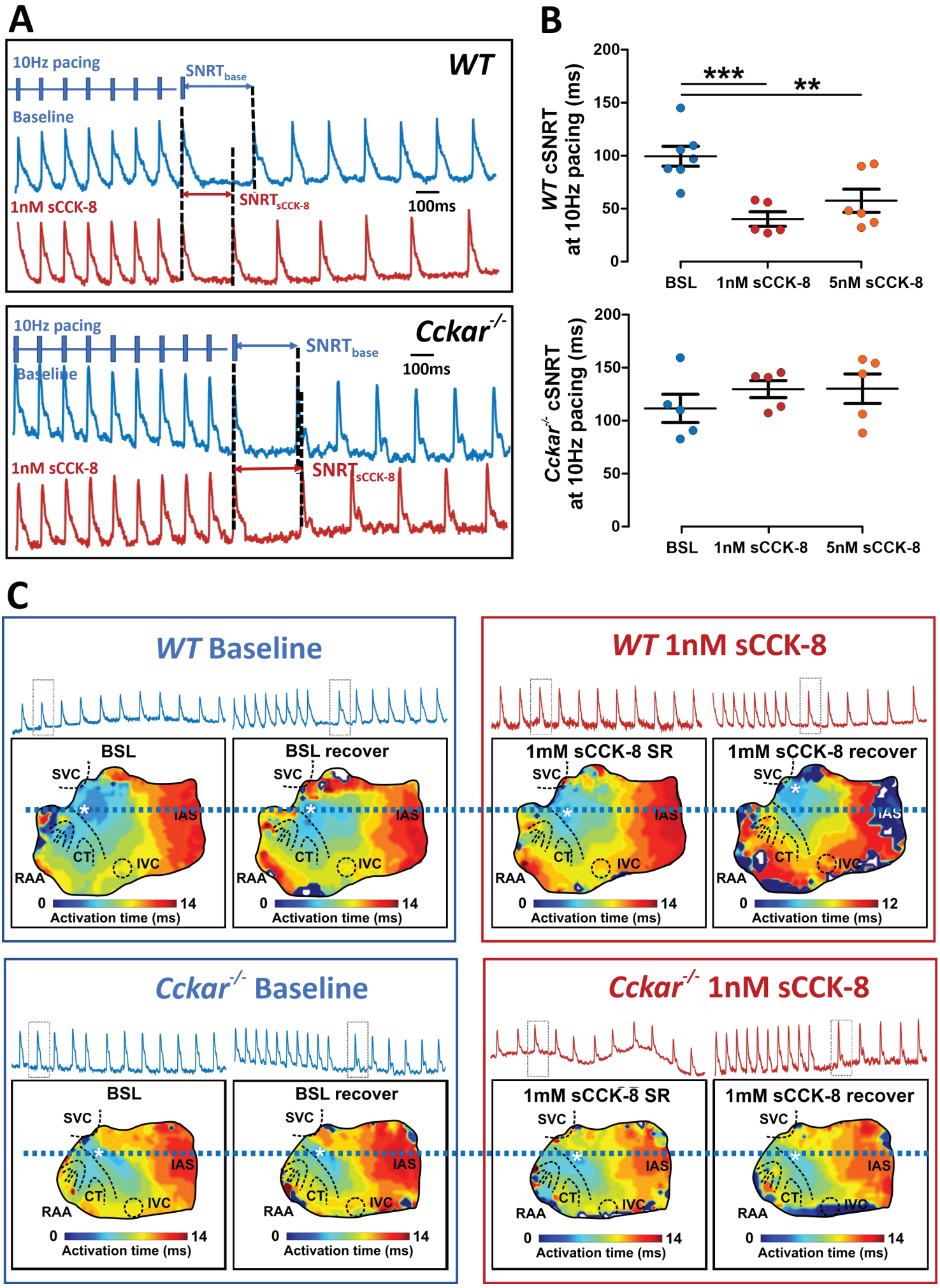
A
10Hz pacing
SNRT base
WT
Baseline
1nM sCCK-8
SNRT sCCK-8
100ms
10Hz pacing
SNRT base
Cckar-/-
Baseline
100ms
1nM sCCK-8
SNRT sCCK-8
B
WT cSNRT at 10Hz pacing (ms)
200
150
100
50
0
***
**
BSL
1nM sCCK-8
5nM sCCK-8
Cckar-/- cSNRT at 10Hz pacing (ms)
200
150
100
50
0
BSL
1nM sCCK-8
5nM sCCK-8
C
WT Baseline
BSL
BSL recover
SVC
IAS
CT
IVC
RAA
0
14
Activation time (ms)
WT 1nM sCCK-8
1mM sCCK-8 SR
1mM sCCK-8 recover
SVC
IAS
CT
IVC
RAA
0
14
12
Activation time (ms)
Cckar-/- Baseline
BSL
BSL recover
SVC
IAS
CT
IVC
RAA
0
14
Activation time (ms)
Cckar-/- 1nM sCCK-8
1mM sCCK-8 SR
1mM sCCK-8 recover
SVC
IAS
CT
IVC
RAA
0
14
Activation time (ms)